Thermal stability of high-k Si-rich HfO2 layers grown by RF magnetron sputtering

Larysa Khomenkova, Xavier Portier, Julien Cardin, Fabrice Gourbilleau

Thermal stability of high-k Si-rich HfO_2 layers grown by RF magnetron sputtering

L Khomenkova[1,2], X Portier, J Cardin and F Gourbilleau[2]

CIMAP, CEA/CNRS/ENSICAEN/UCBN, 6 Boulevard Maréchal Juin, 14050 Caen Cedex 4, France

E-mail: khomenkova@rambler.ru, larysa.khomenkova@ensicaen.fr and fabrice.gourbilleau@ensicaen.fr

Abstract

The microstructure and optical properties of HfSiO films fabricated by RF magnetron sputtering were studied by means of x-ray diffraction, transmission electron microscopy, spectroscopic ellipsometry and attenuated total reflection infrared spectroscopy versus annealing treatment. It was shown that silicon incorporation in the HfO_2 matrix plays an important role in the structure stability of the layers. Thus, the increase of the annealing temperature up to 1000 °C did not lead to the crystallization of the films. The evolution of the chemical composition as well as a decrease of the density of the films was attributed to the phase separation of HfSiO on HfO_2 and SiO_2 phases in the film. An annealing at 1000–1100 °C results in the formation of the multilayer Si-rich/Hf-rich structure and was explained by a surface-directed spinodal decomposition. The formation of the stable tetragonal structure of HfO_2 phase was shown upon annealing treatment at 1100 °C.

(Some figures in this article are in colour only in the electronic version)

1. Introduction

Transition metal oxides and silicates with dielectric constants higher than that of SiO_2 have been considered to replace the silicon dioxide employed in gate dielectric systems of microelectronic devices [1, 2]. In principle, high-k dielectrics allow the reduction of the leakage current and demonstrate good thermal stability, as well as high transparency.

One of the goals for high-k materials is to attain a sufficiently high-quality interface with the Si channel coupled with a stability of the amorphous structure of the gate oxide during deposition. Such a requirement comes from the fact that grain boundaries act as diffusion paths for dopants or oxygen towards the film/substrate interface. Thus, it was observed that post-growth oxidation of pure HfO_2 layers in a $^{18}O_2$ atmosphere at 490–950 °C results in oxygen exchange without increasing the oxygen content in the films [3]. The atomic diffusion of oxygen via oxygen lattice exchange was found to be the predominant diffusion mechanism. When pure HfO_2 films are amorphous and/or nanocrystalline, the diffusion of oxygen is minimized and the excess of oxygen atoms is stabilized as interstitials. The exchange rate increases with temperature due to crystallization of the films [3].

It is known that the dielectric properties of HfO_2 depend significantly on its structure. Amorphous and monoclinic phases exhibit a dielectric constant of about 16–20, but cubic and tetragonal phases have higher relative permittivity (about 28 [4]). From the device application point of view, these latter phases are preferable to the monoclinic one. It was demonstrated both theoretically [5–7] and experimentally [8–10] that the incorporation of cationic dopants in the HfO_2 matrix favors the formation and the stabilization of the tetragonal or cubic phase. At the same time, the dopants have to be chosen to avoid a significant decrease of the band gap energy and dielectric constant of the high-k materials.

The most promising candidate to fulfil these conditions is silicon. For instance, for HfSiO layers grown by atomic vapor deposition [3] it was observed that the Si incorporation in HfO_2 matrix allows the oxygen diffusion from the environment into the films to be controlled. This diffusion was minimized due to the formation of covalent Si–O bonds in comparison with ionic

[1] Permanent address: V Lashkaryov Institute of Semiconductor Physics, 45 Prospekt Nauky, Kyiv 03028, Ukraine.

[2] Authors to whom any correspondence should be addressed.

Hf–O ones and, depending on the Si content, it was completely suppressed. Besides, it was shown that the annealing treatment of such HfSiO films at 490–950 °C results in the formation of SiO_2 close to the film surface that significantly decreases the oxygen diffusion at high temperatures and completely blocks it at low temperatures [3]. On the other hand, the Si incorporation minimizes oxygen exchange inside the film and controls the formation of the SiO_x interfacial layer during the deposition process and post-deposition treatment [3, 11, 12]. Thus, for HfSiO layers grown by atomic vapor deposition, the formation of a SiO_2 interfacial layer was observed at temperatures higher than 600 °C [3], whereas for HfSiO layers grown by RF magnetron sputtering it started at 900 °C [12].

Taking advantage of this Si incorporation in such a matrix, let us turn to consideration of multilayer applications of HfO-based layers. It is known that they can be used as gate and/or control oxides [2]. Besides, HfO_2-based materials with different embedded nanoparticles can be used widely for nanomemory applications [13]. However, the formation of Si nanoparticles usually requires high temperature annealing [14] that can lead to total crystallization of high-k oxide. For example, for HfO_2/Si-rich SiO_2/HfO_2 structures it was shown that the formation of Si nanoparticles was achieved upon annealing at 1100 °C for 1 h, when HfO_2 gate and control oxides were completely crystallized in the monoclinic phase [14]. However, for such structures one can expect that it is possible to use a rapid thermal annealing process to form Si seeds at high temperature in a short time (less than 1 min), and then to decrease the annealing temperature down to the critical temperature value to prevent the crystallization of high-k material during the formation of Si nanoparticles. The latter does not require temperatures as high as 1100 °C (usually 800–900 °C is sufficient), but longer annealing time (about 15–30 min) is necessary. In such a case, the gate material has to be stable during such a treatment.

As we showed earlier [11, 12], hafnium silicate thin films grown by the RF magnetron sputtering approach are homogeneous, amorphous and the thickness of the interfacial SiO_x layer between the high-k layer and the Si substrate does not exceed 1 nm. Moreover, they demonstrate their thermal stability by conserving the amorphous structure after an annealing at temperatures as high as 800–1000 °C for 15 min. Thus, they can be considered as promising candidates for gate materials, especially when higher temperature annealing is required for processing of the device, for example for nanomemory applications.

In addition to the thermal stability of the amorphous phase, the stability of the chemical composition of the high-k silicates is also required. This condition comes from the fact that during the growth process and/or annealing treatment the formation of high-k and low-k regions can occur [15–17]. Most of the studies were performed for Zr silicates. The formation of ZrO_2-rich and SiO_2-rich regions during the growth process was observed whereas the films were found to be amorphous. The alternation of ZrO_2-rich layers with SiO_2-rich layers in the normal direction to the film surface was governed by a driving force that was normal to the film surface. A similar effect was also found for ZrSiO films upon annealing [16].

A similar phenomenon was observed for HfSiO films grown by the atomic vapor deposition technique [17, 18]. The effect of the formation of HfO_2-rich and SiO_2-rich regions in HfSiO materials was explained similarly to that observed for ZrSiO [15, 17]. Unfortunately, no analysis of the crystalline structure of the films versus annealing treatment was reported.

The evolution of the microstructure and chemical composition, as well as the optical properties of the HfSiO materials under annealing treatment is the issue of the present study. The layers, fabricated by RF magnetron co-sputtering of a pure HfO_2 cathode topped by Si chips in a pure argon plasma, were analyzed by means of x-ray diffraction, infrared absorption spectroscopy, spectroscopic ellipsometry and high resolution transmission electron microscopy.

This paper is organized as follows. First, the optical properties of as-deposited and annealed films will be analyzed. The refractive index, thickness and density of as-deposited and annealed films will be extracted from analysis of the spectroscopic ellipsometry data. Next, the obtained results will be compared with the chemical composition and structure of the as-deposited and annealed films. The phase separation stimulated by annealing treatment will be described and a mechanism of this phenomenon will be proposed.

2. Experimental procedure

The HfSiO films were deposited on B-doped Si substrates with a resistivity of 15 Ω cm and the (100) orientation. To remove native oxide the substrates were cleaned in a diluted hydrofluoric solution (10%) and after drying in a nitrogen flow they were immediately placed into the vacuum preparation chamber of the deposition setup. The layers were grown by RF magnetron sputtering of a 4 inch HfO_2 target (99.9%) topped with Si chips in a pure argon plasma. The RF power density, total plasma pressure and substrate temperature were 0.74 W cm^{-2}, 40 μbar and 100 °C, respectively. The Si chips covered 12% of the total surface of the HfO_2 target.

To study the effect of annealing treatment on the layer properties, the samples were annealed under a nitrogen flow in a conventional furnace at different temperatures, T_A = 800–1100 °C, during t_A = 10–30 min.

The combination of non-destructive methods allows information about microstructural and optical properties of the films to be obtained. Thus, infrared attenuated total reflectance (ATR), usually used for thin film investigation, will provide information about the structure and chemical composition of the films. ATR-FTIR spectra were measured in the range 600–4000 cm^{-1} by means of a 60° Ge Smart Ark accessory inserted in a Nicolet Nexus spectrometer. Microstructure properties were analyzed by an x-ray diffraction method using a Phillips XPERT HPD Pro device with Cu Kα radiation (λ = 0.1514 nm) at a fixed grazing incidence angle of 0.5°. An asymmetric grazing geometry was chosen to increase the volume of material interacting with x-ray beam, as well as to eliminate the contribution from the Si substrate.

Spectroscopic ellipsometry was used to determine different parameters of the samples such as optical constants, thickness and surface roughness. The data were collected

by means of a Jobin-Yvon ellipsometer (UVISEL) where the incident light was scanned in the range 1.5–4.5 eV with an incidence angle of 66.3°. The fitting of the experimental data was performed using DeltaPsi2 software [19].

The analysis of film structure versus annealing treatment was completed by TEM observation. Cross-sectional specimens were prepared by a standard procedure involving grinding, dimpling and Ar^+ ion beam thinning until they were electron transparent. The samples were examined by conventional (CTEM) and high resolution electron microscopy (HRTEM) using a FEG 2010 JEOL instrument, operated at 200 kV. Image processing was done with the commercial Digital micrograph GATAN software.

3. Results and discussion

3.1. Spectroscopic ellipsometry analysis

It is known that spectroscopic ellipsometry is a fast, sensitive and non-destructive method for thin film characterization. It requires no special environment and can be easily integrated into semiconductor processing [20, 21].

The spectra consist of the measured Ψ and Δ ellipsometric angles defined from the fundamental equation of ellipsometry

$$\overline{r_p}/\overline{r_s} = \tan\Psi \exp \mathrm{i}\Delta, \tag{1}$$

where $\overline{r_p}$ and $\overline{r_s}$ are the complex reflection coefficients for the parallel and perpendicular polarization of light, respectively. The spectral dependencies of Ψ and Δ can be fitted with appropriate modeling approaches to extract the film thickness and optical constants (refractive index, n, and extinction coefficient, k) based on the best fit between the experimental and simulated spectra [20]. Besides the optical dielectric constant, the surface roughness and film density can also be obtained [21].

Before describing the model used for extraction of the different parameters of the layers, let us recall that the HfSiO layers investigated in the present study were found to be amorphous and homogeneous, in terms of their structural properties and chemical composition, by energy filtered TEM analysis [12]. Moreover, for the as-grown films it was shown that they had a very thin (no more than 1 nm) interfacial SiO_2 layer. This allowed us to consider the as-grown films as a homogeneous medium and to apply the effective medium approximation (EMA) [20, 22] to fit the experimental spectra.

Such an approximation supposes that the macroscopic properties of a medium are based on the properties and the relative fractions of its components. There are several EMA models (Bruggeman, Maxwell–Garnet, etc). They all assume that the macroscopic system is homogeneous (with correlation length below the Lorentz cavity radius) and typical of all mean field theories; they fail to predict the properties of a multiphase medium close to the percolation threshold due to its long-range correlation length. The most frequently considered parameters are conductivity or/and dielectric constant. The Bruggeman effective medium approximation (BEMA) used in this work is defined by the following two equations:

$$\sum_i v_i \frac{\varepsilon_i - \varepsilon}{\varepsilon_i + 2\varepsilon} = 0, \tag{2}$$

and

$$\sum_i v_i = 1, \tag{3}$$

where ε_i and v_i are the complex optical dielectric function and volume fraction for the ith component, respectively. ε is the effective dielectric function corresponding to the measured value for the film.

A four-phase optical model was used to investigate the as-deposited and annealed layers. It consists of the silicon substrate, a SiO_2 interfacial layer, an amorphous HfSiO layer, and a surface rough layer composed of a mixture of void space and HfSiO. It is worth noting that the roughness of the films was estimated to be less than 1.5 nm, as confirmed by film surface observations using atomic-force microscopy. The model structures and optical properties of the films were optimized by least-square refinements (χ^2) from the fit of the experimental data.

To fit spectroscopic ellipsometry data, a dispersion law was chosen based on the Forouhi–Bloomer model (FBM) modified for amorphous semiconductor and insulating materials [23] using an improved parameterization [24]. The dispersion formulae for n and k were given as follows

$$n(\omega) = n_\infty + \frac{B_i(\omega - \omega_i) + C}{(\omega - \omega_i)^2 + \Gamma_i^2},$$

$$k(\omega) = \begin{cases} \dfrac{f_i(\omega - \omega_g)^2}{(\omega - \omega_i)^2 + \Gamma_i^2}, & \omega > \omega_g \\ 0, & \omega \leqslant \omega_g, \end{cases}$$

where

$$B_i = \frac{f_i}{\Gamma_i}(\Gamma_i^2 - (\omega_i - \omega_g)^2),$$

$$C = 2 f_i \Gamma_i (\omega_i - \omega_g)$$

where n_∞ is the refractive index at high frequency, f_i is an oscillator strength, Γ_j is an amortization factor, and ω_i and ω_g are the frequencies of free oscillator.

Two dependencies, $I_s = I \sin 2\Psi \sin\Delta$ and $I_c = I \sin 2\Psi \cos\Delta$, where $I = \frac{E_0}{4}(|r_p|^2 + |r_s|^2)$ and E_0 is the amplitude of electric field of incident light, were fitted. The obtained values of n and k of the as-deposited films are shown in figure 1(a) and (b), respectively. The experimental data and their best fitting are presented in the inset of figure 1(b). n and k values of HfO_2, SiO_2, SiO and bulk Si are also included in figure 1(a) and (b) for comparison.

Usually, Hf silicates are considered as being composed of pure HfO_2 and pure SiO_2 structural units as $(HfO_2)_x(SiO_2)_{1-x}$ and the relative contributions determine the composition of the films [4, 16, 21, 25]. Of HfO_2 and SiO_2, the first has the higher refractive index (figure 1(a)). It is obvious that the n value of HfSiO material must increase with an increase of the HfO_2 fraction, f_{HfO_2}, up to a limit value corresponding to pure HfO_2 (figure 1(a)). In such a case, one can suppose that the k value has to follow this rule too. As one can see in figure 1(b), both oxides are completely transparent in the spectral range of our interest. However, the as-deposited HfSiO sample demonstrates some absorption ability in the 1.5–4.5 eV spectral range, contrary to the data reported in [26]. The

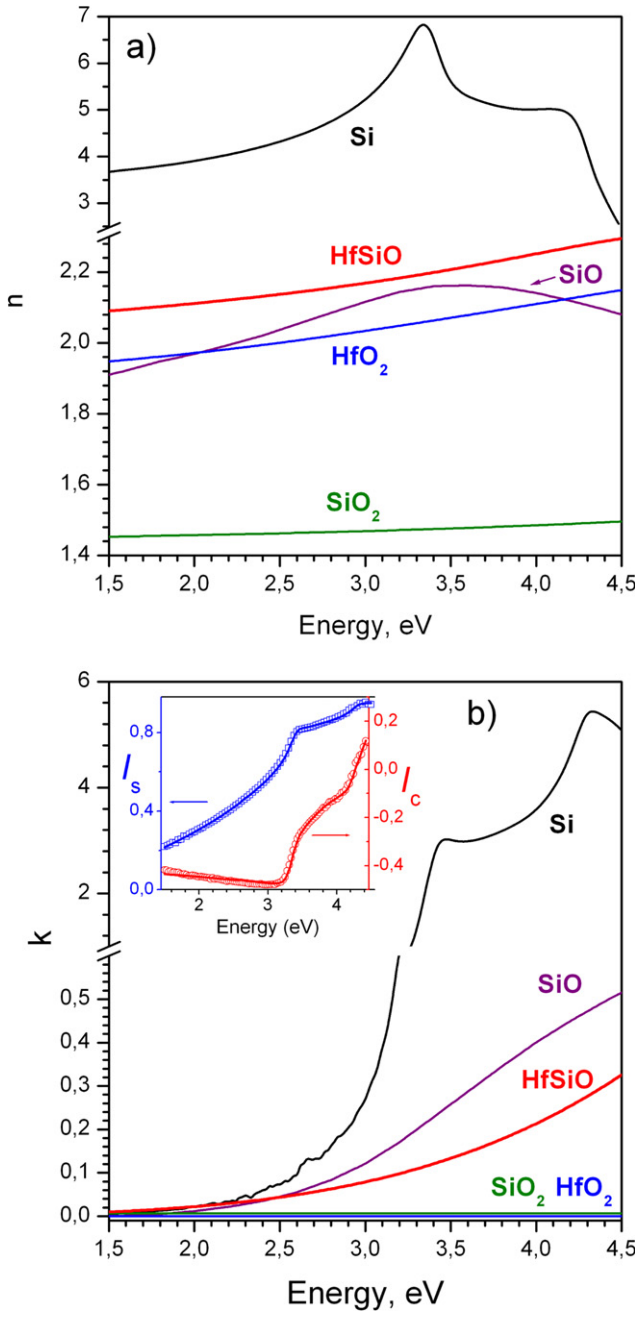

Figure 1. The estimated refractive index, n (a) and absorption coefficient, k (b) of the as-grown HfSiO layer. The inset in figure (b) represents experimental ellipsometry data (symbols) and the fitting curve (solid line) for the as-deposited HfSiO samples. $I_s = I \sin 2\Psi \sin \Delta$ and $I_c = I \sin 2\Psi \cos \Delta$ (Ψ and Δ are the measured ellipsometry parameters). The $n(E)$ and $k(E)$ dependencies for pure HfO_2, SiO_2, SiO and bulk Si are also presented.

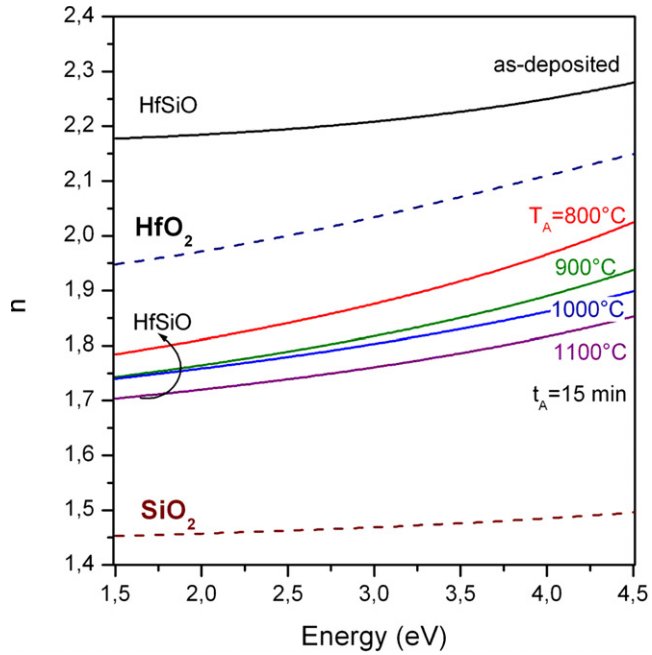

Figure 2. The calculated refractive index, n, for as-deposited films and those annealed at 900–1100 °C for 15 min, grown at RFP = 0.74 W cm^{-2}. The n variation for both pure HfO_2 and pure SiO_2 materials are also shown by dashed lines.

comparison of the absorption properties of SiO_2, SiO and bulk Si reveals that SiO_2 is transparent in this spectral range, while Si suboxides and bulk Si demonstrate high enough absorption (figure 1(b)). Thus, one can speculate that the absorption in the as-deposited HfSiO films occurs due to a presence of the SiO_x phase instead of SiO_2. On the other hand, it is possible to assume that the absorption could be due to the formation of a HfSiO network which cannot be considered as a mixture of HfO_2 and SiO_2 phases alone. However, since Hf ions are less electronegative than Si ones, it is obvious that the formation of HfO_2 structural units is preferable to SiO_2 ones and consequently, the formation of the SiO_x phase is possible. This could explain the behavior of the extinction coefficient k in the as-deposited layers (figure 1(b)).

The analysis of the annealed films shows a gradual decrease of n with annealing temperature (figure 2). Furthermore, k decreases and a shift of the 'absorption edge' to higher energy was observed, which could be evidence of the increased transparency of the films after the annealing treatment (not shown here). The data obtained can be explained by the difference in the structure and in the composition of the as-deposited and annealed films.

It is known that the refractive index of pure HfO_2 increases with the annealing temperature due to the crystallization process [27]. In our case, the n decrease could be explained by the formation of pores and/or by the increasing contribution of the SiO_2 phase. The latter could be due to oxygen diffusion into the films during the annealing treatment resulting in the formation of a thicker interfacial SiO_2 layer. Both these facts would be a reason for the decrease of n and k values.

However, as we showed earlier [11, 12], after annealing at 800 °C for 15 min, the films kept their amorphous structure without any pore formation. Moreover, the thickness of the interfacial SiO_2 layer did not exceed 2 nm; so they cannot be the only reasons for such a decrease of the refractive index. Thus, another fact has to be taken into consideration, for example a higher contribution of SiO_2 phase in the film due to phase separation and formation of HfO_2 and SiO_2 phases.

Further increasing the annealing temperature up to 1100 °C results in a decrease of the n and k values (figure 2).

Table 1. The physical and optical parameters of HfSiO samples versus annealing treatment.

Parameters		Annealing temperature (°C)				
		25	800	900	1000	1100
Thickness (nm)	HfSiO layer	17.15	17.3	20.46	21.05	22.54
	SiO_2 interfacial layer	1.03	1.06	2.73	3.32	5.0
Refractive index, n	at 1.5 eV	2.081	1.790	1.743	1.740	1.704
Polarizability, α (bohr^3)	α_{HfO_2} for HfO_6 units			35.28 [4]		
	α_{HfO_2} for HfO_8 units			32.21 [4]		
	α_{SiO_2} for SiO_4 units			19.68 [4]		
	α_{HfSiO} for HfO_6/SiO_4	33.25	30.61	29.82	29.04	28.26
	α_{HfSiO} for HfO_8/SiO_4	30.58	28.45	27.82	27.20	26.57
Fraction of HfO_2	f_{HfO_2}	0.87	0.70	0.64	0.60	0.55
Density for (g cm^{-3})	ρ_{HfSiO} for HfO_6/SiO_4	8.02	6.08	5.56	5.55	5.21
	ρ_{HfSiO} for HfO_8/SiO_4	8.72	6.54	5.94	5.92	5.54

At the same time, if HfO_2 crystallization occurs at higher temperatures, the n and k decreases will be due to the more important contribution of the SiO_2 phase. As one can see from table 1, an annealing treatment leads not only to the increase of the interfacial layer thickness but also to the increase of the thickness of the HfSiO layer itself. Such an expansion can be caused by a further increase of the contribution of the SiO_2 phase which has higher lattice parameter than HfO_2 and must affect the density of the films.

3.2. *Effect of annealing treatment of the density of the films*

The density of the films can be estimated using the Clausius–Mossotti relationship between optical dielectric constant and film density, ρ, given by equation (4)

$$\frac{\varepsilon - 1}{\varepsilon + 2} = \frac{4\pi}{3}\frac{\bar{\alpha}}{\bar{V}}, \tag{4}$$

where $\bar{V}$ is the average structure unit volume and polarizability $\bar{\alpha}$ can be considered as a local and additive quantity in the contrast with ε. The film being composed by different phases, its density, ρ, can be considered as $\sum_i v_i \rho_i = \rho$, where ρ_i is the density of the ith component, one can extract the ρ value, using equation (4) rewritten as

$$\frac{n^2 - 1}{n^2 + 2} = \frac{4\pi}{3}\left(\frac{N_A \rho}{M}\right)\bar{\alpha}, \tag{5}$$

where M is the molar mass and N_A is Avogadro's constant, taking into account that $\varepsilon = n^2$. In such a case, the refractive index is taken from the fitted parameters, while the polarizability was estimated based on the values available for Hf silicate materials [4].

To estimate the value of ρ, we have to use an appropriate value of the polarizability, α. This is an important parameter for mixed media. It has additive properties, contrary to the dielectric constant, that allow it to be estimated using the known polarizabilities of HfO_2 and SiO_2 phases and their contribution to the HfSiO film following the equation (6)

$$\bar{\alpha}_{HfSiO} = f_{HfO_2}\alpha_{HfO_2} + f_{SiO_2}\alpha_{SiO_2} \tag{6}$$

where f_{HfO_2} and f_{SiO_2} are the volume fractions of HfO_2 and SiO_2, α_{HfO_2} and α_{SiO_2} are the corresponding polarizabilities. The α_{HfSiO} values can be calculated for different HfO_2 contents in the matrix. We have also to know f_{HfO_2} and f_{SiO_2} for our films. One possibility to get information about the contribution of both phases is to examine the theoretical dispersion of the refractive index of HfSiO materials versus HfO_2 content and to compare these results with the experimental ones presented above. After getting both parameters, n and α_{HfSiO}, we can estimate the density of the films, ρ.

3.2.1. Dispersion of the refractive index for HfO_2-based systems. First of all, we estimate the f_{HfO_2} value. We consider HfSiO material as a two-phase system. One of them is HfO_2. The other one is often assumed to be SiO_2. However, we can assume that incorporation of Si into the HfO_2 matrix can occur as SiO_x and/or Si itself since the layers investigated were grown by sputtering of a HfO_2 target topped by pure Si chips. Thus, the Si-based phase was assumed to be SiO_2, or SiO, or Si to simplify the modeling. The dispersion of the refractive index in 1.5–6 eV spectral range was estimated for three different Si-rich HfO_2 media versus the contribution of each phase. The results versus HfO_2 content are shown in figure 3(a) and (b) only at 2 eV since they are representative over the whole spectral range.

As one can see, n values increase with f_{HfO_2} for the case of the HfO_2/SiO_2 medium, while it decreases for the HfO_2/SiO and HfO_2/Si media. To compare these results with experimental n values obtained for as-deposited films, we added the latter to the figure 3(a). Since it was only one value $n = 2.21$, we added it as a straight line. The intersection of this line with the calculated curves gives the possibility to estimate the f_{HfO_2} value for the as-deposited films. As one can see, the experimental n value exceeds the values calculated for HfO_2/SiO_2 and for HfO_2/SiO media. In such a case, it should be possible to consider that the Si-based phase is incorporated as amorphous Si itself. However, comparing the electronegativity of elements present in HfSiO material, it is obvious that the formation of Hf–O and Si–O bonds is more likely to occur than Hf–Si and Si–Si bonds, whereas Si–O bonds are more probable than Si–Si bonds. As a consequence, the Si-based phase is presented as SiO_x with $0 < x < 1$. Such an assumption could explain the high n value obtained for the as-deposited films (figure 3(a)).

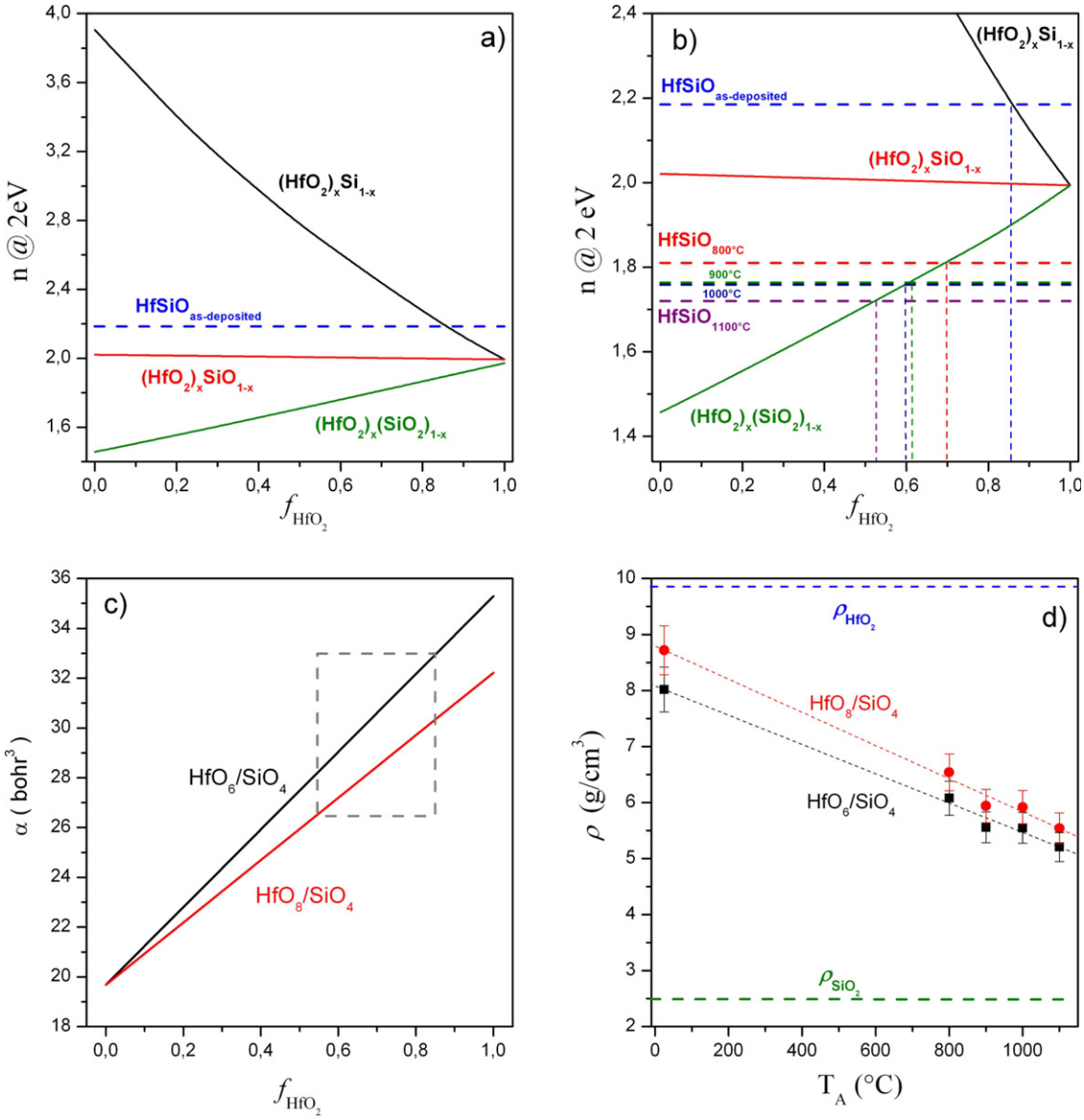

Figure 3. (a) Calculated refractive index for $(HfO_2)_x(Si)_{1-x}$, $(HfO_2)_x(SiO)_{1-x}$ and $(HfO_2)_x(SiO_2)_{1-x}$ versus HfO_2 content, f_{HfO_2}, using the Bruggemann EMA model. The refractive index for as-deposited samples is shown by the dashed line. All the data are taken for 2 eV light energy. (b) Comparison of calculated refractive indexes for $(HfO_2)_x(Si)_{1-x}$, (1), $(HfO_2)_x(SiO)_{1-x}$ (2) and $(HfO_2)_x(SiO_2)_{1-x}$ with experimental values obtained for as-deposited ($HfSiO_{AD}$) and annealed films (from $HfSiO_{800\,°C}$ to $HfSiO_{1100\,°C}$) represented by straight lines. The horizontal dashed lines represent the experimental n values whereas the corresponding vertical dashed lines show the possible volume fraction of HfO_2 in the films, considering results for the n and chemical composition obtained by the ATR method. All the data are taken for 2 eV light energy. (c) The polarizability, α, calculated using equation (6) for different HfO_2 content in HfSiO films using the approach described in [4]. The dashed line frames the range of the polarizability for the films versus HfO_2 content estimated from the corresponding refractive index data. (d) The estimated density of as-deposited films and films annealed at 800–1100 °C for 15 min (for the film composed by HfO_6/SiO_4 and HfO_8/SiO_4 structure units). The densities of SiO_2 and HfO_2 are also presented for comparison.

The experimental data obtained for annealed films are presented similarly in figure 3(b) that is a frame of figure 3(a). It is seen that the refractive index of the annealed films is less than that calculated for the HfO_2/SiO medium. This means that for the annealed samples, the Si-based phase can be considered as SiO_x with $x > 1$ for any f_{HfO_2} values. Since the best modeling results were found for the HfO_2/SiO_2 medium (figure 3(b)), we estimate the f_{HfO_2} based on this dependence. One can see that f_{HfO_2} decreases with annealing treatment from 0.7 ($T_A = 800\,°C$) to 0.55 ($T_A = 1100\,°C$). For the as-deposited films, $f_{HfO_2} \leqslant 0.86$ (figure 3(b)) and the upper limit can be overestimated, but its lower limit was not less than 0.7. To calculate the maximum density of the as-deposited films we used $f_{HfO_2} = 0.86$.

We obtained information about the refractive index and the contribution of the HfO_2 phase. To finalize the estimation of the density of as-deposited and annealed films, we have to determine the polarizability of the films.

3.2.2. Polarizability of HfSiO films. It is known that HfO_2 can be presented by HfO_4, HfO_6 and HfO_8 structure units [4], but the most probable ones are HfO_6 and HfO_8. Among these, the

highest value of α_{HfO_2} is 35.28 bohr^3 corresponding to HfO_6 structure units. However, in the case of HfSiO materials, it was shown that HfO_8 units prevail, giving $\alpha_{HfO_2} = 32.21$ bohr^3 [4]. Since both types of structure units can compose HfSiO films, we will consider that the HfO_2 phase is built by HfO_6 or HfO_8 units that will give us the lower and upper limits of the density of the films. For the case of the SiO_2 phase, it is usually composed of SiO_4 and SiO_6 units [4]. At the same time, it was shown that for the case of high-k silicates, SiO_4 units are the most probable structural elements [4] corresponding to $\alpha_{SiO_2} = 19.68$ bohr^3.

Thus, based on the assumption that our films are composed of HfO_8/SiO_4 or of HfO_6/SiO_4 structure units, we calculated the values of polarizability versus HfO_2 content for HfSiO films using equation (6). The results are presented in table 1 and in figure 3(c). As one can see, α_{HfSiO} decreases with the annealing treatment (table 1) from 33.25 down to 28.26 bohr^3 for the case of HfO_6/SiO_4 and from 30.58 to 26.57 bohr^3 for HfO_8/SiO_4.

Thus, we can turn now to the estimation of the density of the films.

3.2.3. Density of the films. Taking into account equation (5) and using the α_{HfSiO} and n values, we estimated the density of the films. The results are given in table 1 and in figure 3(d). The decrease of the film density is clearly seen. Using both types of media we found that the density of the as-deposited films is in the range of 8–8.7 g cm^{-3}. This value can be overestimated due to uncertainties in the estimation of the HfO_2 fraction in the as-deposited films based on the refractive index data. At the same time, they demonstrate an agreement with the data of [21]. The density of the films decreases from 6.1–6.5 to 5.2–5.5 g cm^{-3} when the annealing temperature increases from 800 up to 1100 °C (figure 3(d)).

It is worth noting that the film density was obtained for the HfSiO layer itself. The model used for the fitting of ellipsometry spectra allowed us to eliminate the contribution of the interfacial SiO_2 layer in the optical parameters of annealed films. In this case, the decrease of the density of the films can be explained by the increasing contribution of a low density phase. The SiO_2 phase is one of the most probable candidates to explain the decrease of the density of the films annealed at 800 °C since, as shown earlier, such an annealing did not lead to a significant transformation of the film structure [12]. However, the decrease of the film density at higher annealing temperatures could be due to a gradual increase of the contribution of the SiO_2 phase as well as pore formation. Note that even if the HfO_2 phase formed under annealing, its density increases usually [27] due to its crystallization. To discriminate the reasons responsible for the variation of the film density, the analysis of the chemical composition as well as structure properties of the films was performed for the same samples by ATR and XRD methods, whereas the TEM study was used to obtain information, not only about the presence of pores, but also to get an answer as to whether the phase separation occurs over the film thickness.

3.3. ATR spectra of as-deposited and annealed layers

Among non-destructive methods to study thin films, the ATR technique holds an important place, since it allows very thin layers to be analyzed. Unfortunately, referenced ATR data for HfSiO materials are not so numerous. The only known data are those regarding the monoclinic HfO_2 phase, while for tetragonal and cubic phases of HfO_2 and, moreover, for $HfSiO_4$ they are not available in the case of ultrathin films.

The interpretation of experimental data obtained for high-k silicate materials is usually based on the comparison of infrared spectra obtained for amorphous SiO_2 and HfO_2, and their transformation due to an increase of the high-k material contribution.

The continuous random network of SiO_2 consists of corner-coordinated SiO_4 tetrahedra, and the disorder of the amorphous structures comes from the Si–O–Si bond angle changes. Usually, SiO_2 demonstrates three main peaks in the mid-infrared range, coming mainly from the motion of oxygen atoms, and under specific conditions several LO and TO phonons of the Si–O bond can be detected in the 450–1350 cm^{-1} spectral range: at 1076 cm^{-1} (TO_3) and 1256 cm^{-1} (LO_3), at 1160 cm^{-1} (TO_4) and 1200 cm^{-1} (LO_4), at 810 cm^{-1} (TO_2) and 820 cm^{-1} (LO_2), as well as at 457 cm^{-1} (TO_1) and 507 cm^{-1} (LO_1) [28, 29]. It is known that the decrease of SiO_2 layer thickness to nanometer scale is accompanied by a shift of the peak positions of all vibration bands to lower wavenumbers, as well as a decrease of the intensity of TO_4–LO_4 phonons that are usually considered as a feature of the disordering of the SiO_2 matrix [29]. In the case of LO_3 and TO_3 phonons this shift is about 25–30 cm^{-1} [30]. However, the detection of the LO_3 phonon is usually considered as evidence of the formation of a perfect Si/SiO_2 interface [31].

The typical ATR spectrum of SiO_2 film, having a similar thickness to the studied HfSiO films, is presented in figure 4(a). Two Si–O vibration bands, peaked at about 1060 cm^{-1} (TO_3 phonon) and at about 815 cm^{-1} (TO_2 phonon), are revealed in the 600–1350 cm^{-1} spectral range. The difference in the observed peak positions for Si–O bands in comparison with the corresponding values mentioned above is due to the film thickness [29].

ATR spectra of as-deposited HfSiO layers demonstrate the presence of a broad band peaked at 1050 cm^{-1} with a shoulder at about 900 cm^{-1} with a tail up to 600 cm^{-1} (figures 4(a) and (b)). The broadening of Si–O vibration bands as well as the shift of their peak positions to lower wavenumbers is due to the Hf incorporation into the SiO_2 matrix. The latter modifies the SiO_2 network due to the higher Hf–O bond length (1.96–2 Å) in comparison to the Si–O one (1.6 Å). The shape of the ATR spectrum (figure 4) gives evidence of the formation of an amorphous network of a binary compound in the as-deposited films.

An annealing of the layers at $T_A = 800$ °C for 15 min leads to an increase of the intensity as well as to the slight narrowing and to the shift of the broad ATR peak from 1050 to 1070 cm^{-1}. By contrast, the lower wavenumber part of the ATR spectrum is featureless (figure 4). A further increase of the temperature up to $T_A = 1000$ °C results in a continuous

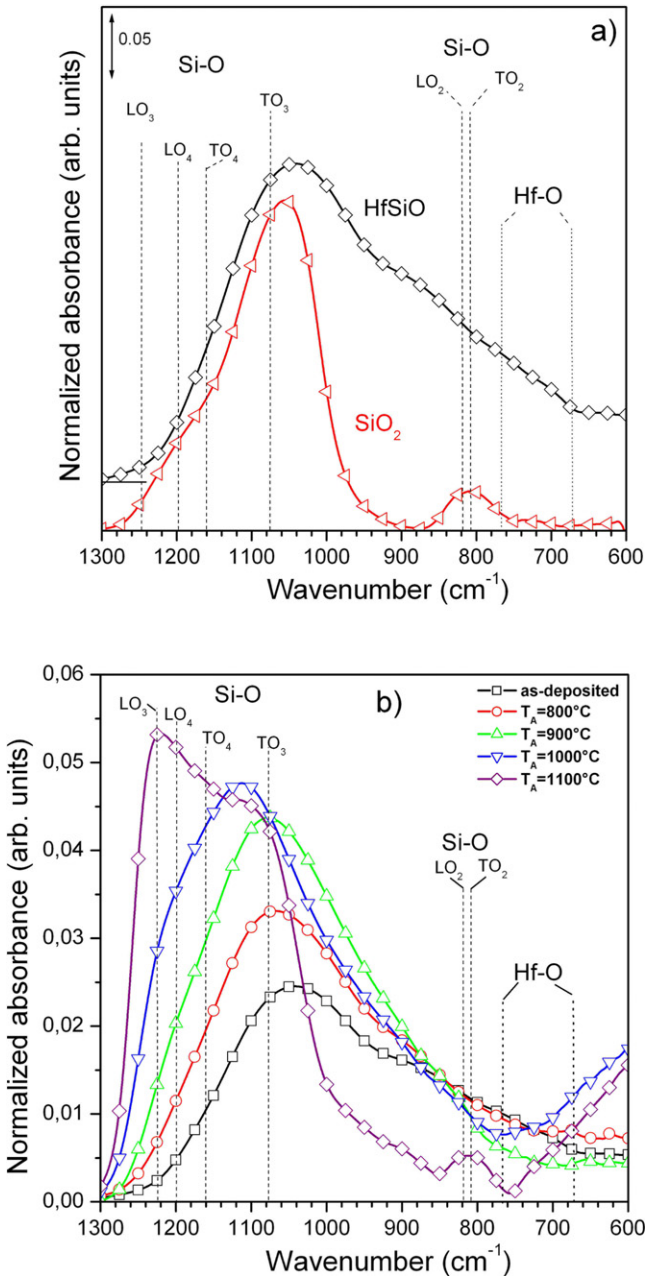

Figure 4. (a) Comparison of ATR spectra of HfSiO and SiO_2 thin films. The thickness of both films is about 18 nm. The vertical dashed lines show the peak positions of all vibration bands observed for the SiO_2 and HfSiO layers. (b) Evolution of ATR spectra with annealing treatment of the HfSiO layer at 800–1100 °C. The annealing time is 15 min.

increase of the peak intensity, to the shift of the peak position to 1120 cm^{-1} and to the appearance of a shoulder at about 1220 cm^{-1}. A treatment at $T_A = 1100$ °C causes the narrowing of this vibration band, a redistribution of the intensities of its components and the appearance of a band at about 820 cm^{-1}.

All these three bands can be ascribed to the SiO_2 phase, as observed for the SiO_2 film (figure 4(a)). The intensity increase and the peak shift to higher wavenumbers can be explained by the increasing contribution of the SiO_2 phase in the film structure as well as by a realignment of the Si–O bonds followed the SiO_2 phase formation. The latter could be due to the formation of an interfacial SiO_2 layer confirmed by the higher intensity of the LO_3 phonon exceeding the TO_3 one (figure 4(b)). At the same time, the contribution of TO_3 and TO_4–LO_4 phonons to the ATR spectrum enables us to assume the presence of a SiO_2 phase in the film due to the phase separation inside the HfSiO film into SiO_2 and HfO_2 phases.

The phase separation under annealing at $T_A = 1000$ and 1100 °C is confirmed by an increase of the ATR intensity in the range of 780–600 cm^{-1}, corresponding to Hf–O vibrations. Usually, two vibration bands peaked at 770–780 cm^{-1} and 680 cm^{-1}, and coming from the HfO_2 monoclinic phase, can be found in this spectral range [32–34], whereas a broad and featureless band is ascribed to amorphous HfO_2 [11, 12]. We suppose that this increase of the ATR band intensity corresponds to the HfO_2 phase formation. However, it is hardly believable that such a high annealing temperature (1100 °C) could lead to an amorphous HfO_2 phase. To get more information about the structure of the HfO_2 phase, we performed a XRD study for these samples.

It is worth noting that the absence of any transformation of the ATR band in the range 780–600 cm^{-1} during annealing at T_A up to 900 °C gives evidence that the incorporation of silicon into an HfO_2 matrix improves the thermal stability of the layers. The most probable reason is that the high flexibility of the Si–O bonds allows the amorphous nature of fused silica to be conserved. However, even if HfSiO could be stable at such an annealing temperatures, the transformation of the Si–O vibration band might be due to a better silicon oxide structure and/or due to the formation of a SiO_2 interfacial layer. Such a transformation occurs at lower temperatures (less than 900 °C) than the phase separation in the HfSiO film (1000–1100 °C). To clarify this issue, we performed TEM observations of cross sections of the samples which we will present below.

3.4. XRD study of HfSiO films

To obtain information about the phase separation caused by high temperature annealing and about the HfO_2 structure, an XRD study has been performed on the samples described above.

It is worth noting that most of the crystallographic data for HfO_2-based materials found in the literature are for monoclinic HfO_2 and tetragonal $HfSiO_4$ phases. The data for other HfSiO compounds are rare and in most cases they were interpreted based on results obtained for bulk HfO_2 and $HfSiO_4$ materials.

In figure 5, the XRD pattern for as-deposited films shows a broad peak in the range of $2\Theta \approx 25°$–$35°$ with a maximum intensity located at $2\Theta \approx 32°$. This result demonstrates the amorphous nature of as-deposited layers. An annealing at temperatures as high as $T_A = 800$–900 °C for 15 min does not lead to a transformation of the shape of this broad peak. The appearance of two overlapped peaks at $2\Theta \approx 30.3°$ and 35.3° occurs after annealing at $T_A = 1000$ °C. The increase of annealing temperature results in an increase in the intensity of these peaks with their concomitant narrowing, as well as the appearance of other peaks in the range of $2\Theta = 40°$–$65°$ at $2\Theta \approx 50.6°$ and 59.8°. Note that the peak at $2\Theta \approx 55°$

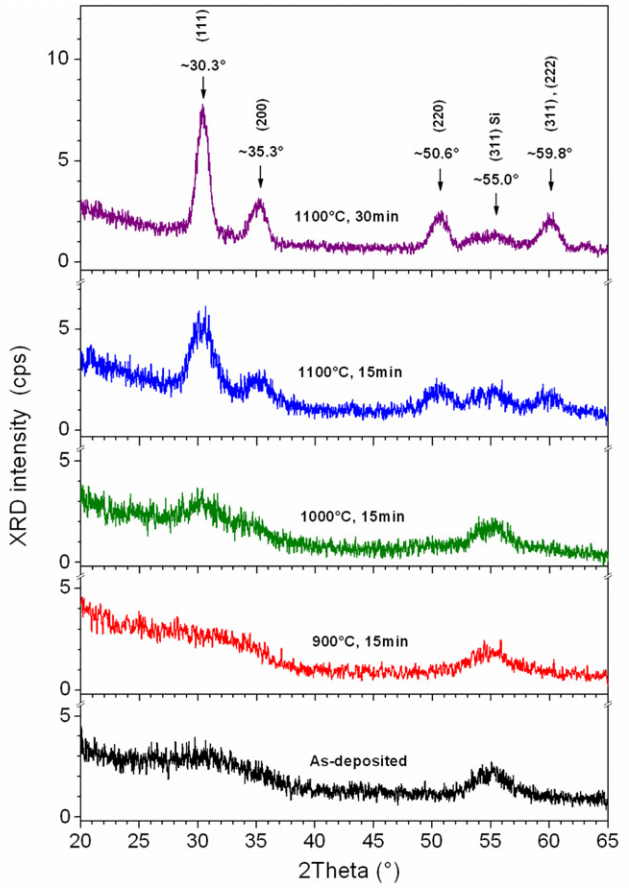

Figure 5. XRD patterns of as-deposited and annealed HfSiO layers. Annealing parameters are mentioned for each spectrum in the figure.

observed for all the samples is due to the Si substrate. The layer annealed at $T_A = 1100\,°C$ for 15 min shows the most intense XRD peaks at $2\Theta \approx 30.3°$, $2\Theta \approx 35.3°$ and $2\Theta \approx 50.6°$ corresponding to the (111), (200) and (220) planes of the tetragonal HfO_2 phase, respectively. The peak at $2\Theta \approx 59.8°$ can be considered as a overlapping of the reflections from the (311) and (222) planes of the same phase.

Usually the tetragonal phase of HfO_2 is observed for ultrathin films, while the annealing treatment at temperatures as high as 800 °C favors its transformation to the monoclinic phase [35]. However, in our case, a longer annealing treatment (up to 30 min) at $T_A = 1100\,°C$ results in an increase of the intensities of only the observed XRD peaks and does not lead to the appearance of other peaks. This could be evidence of the thermal stability of the tetragonal HfO_2 phase in our samples. Since it has higher dielectric constant in comparison with that of the monoclinic phase, such a film can be used as a gate material for structures needing a high temperature annealing process, for example, for some nanomemory structures with embedded Si nanoparticles [14].

One of the important results obtained from comparison of our XRD data with ATR spectra measured for the same samples, is the fact that the increase of intensity of ATR band in the spectral range of 600–780 cm^{-1} is due to the HfO_2 phase formation, which begins mostly at $T_A \geqslant 1000\,°C$. However, the absence of a well-defined peak at 770–780 cm^{-1} demonstrates that our samples do not contain the monoclinic HfO_2 phase, while they cannot be considered as amorphous only. As we showed above, the formation of the tetragonal HfO_2 phase is also possible, leaving the low wavenumber part of the ATR spectra as featureless. In such a case, a combination of both techniques is required to obtain the information about the structure of the HfSiO films.

The analysis of the optical properties of the layers showed a decrease of their refractive index with annealing treatment. Regarding the structural properties, the phase separation is confirmed by ATR spectra, whereas the crystallization of the HfO_2 phase is demonstrated by the XRD data. Since an increase of refractive index is expected with HfO_2 crystallization, one can conclude that the continuous n decrease occurs due to an increasing contribution of the SiO_2 phase. At the same time, neither ATR nor XRD studies can reveal unambiguously where this SiO_2 phase is located, i.e. at film/substrate interface or embedded in the film itself. However, based on these results and on the estimation of the film density, we can assume the presence of the SiO_2 phase inside the volume of the HfSiO layer. The latter will be confirmed by TEM analysis of the as-deposited and annealed films.

3.5. TEM analysis of the structural properties of the films

TEM images of the cross sections of as-deposited and annealed samples are shown in figure 6. As-deposited samples are homogeneous, smooth enough and do not have a thick interfacial layer (its thickness not higher than 1 nm). These observations corroborate the results obtained by fitting of ellipsometry spectra. The increase of the annealing temperature up to 900 °C leads to an increase of total film thickness. However not only an increase of the interfacial SiO_2 layer thickness, but also an expansion of the HfSiO film itself occurs (figure 6(b)). The appearance of bright and dark alternate lines parallel to the film/substrate interface is seen and can be explained by the Hf segregation process, whereas the film stays amorphous (figure 6(b)). A further increase of annealing temperature up to 1000 °C results in the formation of a thicker SiO_2 interfacial layer as well as in a greater contrast between the bright and dark regions (figure 6(c)). They correspond to SiO_2-rich and HfO_2-rich phases that are evidence of the HfSiO phase separation. Also, the crystallization of a HfO_2 phase begins to appear. Upon annealing at 1100 °C, an increase of the SiO_2 interfacial layer thickness (up to 5 nm) is seen. The crystallization of the HfO_2 phase is more pronounced (figure 6(d) and (e)). The crystallites are mainly located in the dark regions as demonstrated by figure 6(e) which is an enlargement of the squared region shown in figure 6(d).

The evolution of the interfacial SiO_2 layer thickness as well as that of the entire film confirm the values obtained by fitting of ellipsometry spectra (table 1).

Figure 6(f) represents a typical selected area electron diffraction (SAED) pattern corresponding to the film and a part of the [110] oriented silicon substrate. Apart from the well-defined dots coming from the silicon substrate, four weak

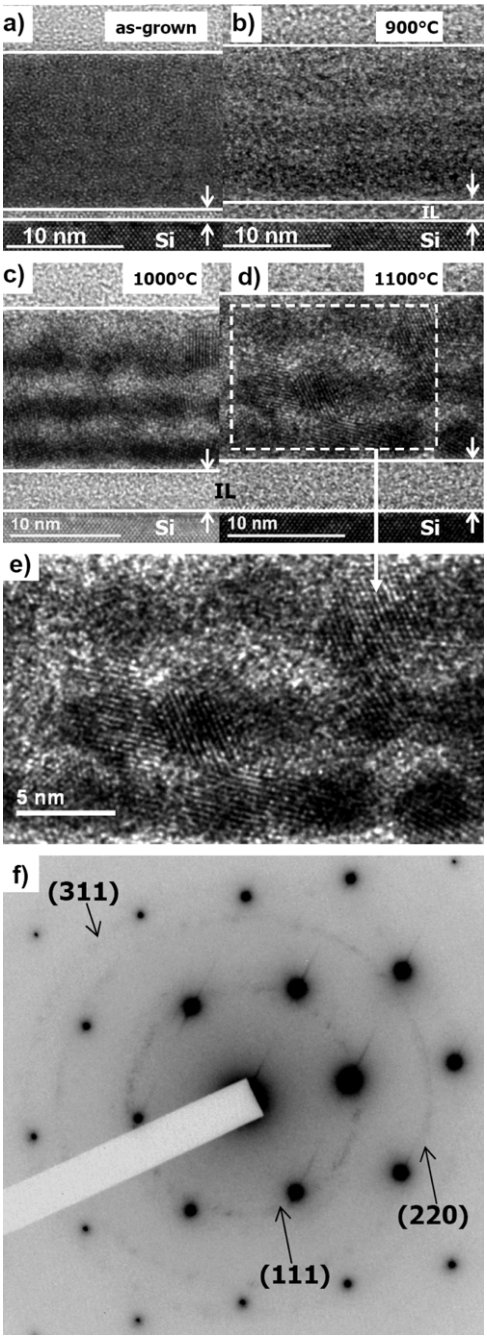

Figure 6. TEM cross sections of the HfSiO layer taken for as-deposited (a), annealed at 900 °C (b), 1000 °C (c) and 1100 °C (d) in N_2 flow for 15 min. The electron diffraction pattern is shown for the sample annealed at 1100 °C. IL is the interfacial layer.

rings appeared, as marked in figure 6(e). The lattice plane distances estimated from SAED were 2.95, 1.80 and 1.53 Å. These distances are compatible with lattice planes of the HfO_2 tetragonal phase: $d_{[111]} = 2.95$ Å, $d_{[220]} = 1.82$ Å and $d_{[311]} = 1.59$ Å.

It is known that thick pure HfO_2 usually has the monoclinic phase, whereas tetragonal and cubic phases appear at 1670–2200 °C [35]. When the thickness of the layer decreases to the nanometer scale, the presence of the tetragonal phase can be observed in pure HfO_2 layers [36]. However, it transforms easily to the monoclinic phase at moderate temperatures [36]. TEM observations of HfSiO films show that the tetragonal phase is stable in such films under annealing at 1100 °C and such films can be used for applications that need high temperature annealing [14].

The appearance of bright (SiO_2-rich) and dark (HfO_2-rich) regions without crystallization of the films (at 900 °C, figure 6(b)) can be explained by a diffusional spinodal decomposition [16, 17] that requires an external field or sources. The latter could be the difference in free energies between the film volume and the film/substrate interface or film surface. For ultrathin films, both of them play an important role in the film decomposition and surface-directed spinodal decomposition was predicted for thin silicate films.

It is known that the Si–O bond is covalent, whereas the M–O (M = Ti, Zr, Hf) is ionic, giving rise to a metastable miscibility gap in high-k silicates. They are usually strained, and a decrease of their free energy is predicted through a phase separation process [37]. The appearance of SiO_2 and MO_2 phases occurs due to lowering of the coordination of silicon and metal cations. The reduction of the Si–Si and Si–O distances and the lowering of Si coordination occur faster than the lowering of metal cation coordination and an optimization of the M–M distance. This is due to an energetic barrier for movement of metal cations through the O sub-lattice caused by the ionic behavior of M–O bonds [37]. At the same time, this barrier is lowered at elevated temperatures and favors the formation of MO_2 nuclei followed by the growth of crystallites around them [37].

A similar film decomposition was observed in previous works for ZrSiO films [15, 25]. It was shown that $(ZrO_2)_x(SiO_2)_{1-x}$ films with $x = 0.1$–0.6 decompose into ZrO_2-rich and SiO_2-rich phases under annealing at 900 °C. The alternation of ZrO_2-rich layers with SiO_2-rich ones was formed in the direction normal to the surface. The nature of the layer closest to the film/substrate interface (i.e. ZrO_2 rich layer or SiO_2 one) depends on the total thickness of the film [25]. Above a critical thickness, the ZrO_2 layer can be localized at the film/substrate interface as well as near the film surface, leading to the formation of a multilayer structure.

It was shown that the mechanism of phase separation of HfSiO films is also a *surface-directed* spinodal decomposition. This effect was demonstrated in films fabricated by the atomic-layer deposition technique [16, 17]. It was shown that, usually, a very thin SiO_2 layer (about monolayer of SiO_2) is located near the film surface, whereas beneath it a Hf-rich layer was observed. For films thinner than 5 nm, a Hf-enrichment of the top layer of the film occurs during the growth process due to the diffusion of Hf towards the film surface, while a Si-rich layer forms close to the film/substrate interface. For thicker films, the formation of an alternating Si-rich/Hf-rich structure was found and explained by the diffusion of Hf ions towards the substrate. However, films thicker than 10 nm lose their layered structure in the middle of the film [16, 17]. It was shown that rapid thermal annealing of such films results in the formation of a layer structure, while longer annealing time led to the formation and crystallization of the HfO_2 phase. Unfortunately, this study was performed only for

$(HfO_2)_{0.25}(SiO_2)_{0.75}$ films [16, 17] without detailed analysis of the crystalline HfO_2 structure.

Considering the fact that the decomposition of $(ZrO_2)_x(SiO_2)_{1-x}$ films was studied for $x = 0.1$–0.6 and the properties of $(HfO_2)_{0.25}(SiO_2)_{0.75}$ were found to be similar to Zr silicates with a close composition, one can admit that Hf and Zr silicates have similar properties over a wide range of x. In such a case, the mechanisms responsible for the phase separation in both silicates have to be the same.

Based on the results presented above, we can assume that the formation of HfO_2-rich and SiO_2-rich layers in our films during the annealing treatment is also governed by a surface-directed spinodal decomposition. Annealing at moderate temperatures results in a diffusion transformation of the layer composition leading to the formation of HfO_2-rich and SiO_2-rich regions without crystallization of the films. This was observed at $T_A = 800\,^\circ$C in [14] and demonstrated in figure 6(b) for $T_A = 900\,^\circ$C. The further increase of the annealing temperature and/or time governs the HfO_2 phase crystallization, as is demonstrated by figures 5 and 6(c) and (d).

TEM study showed also the increase of the total thickness of the film stimulated by annealing treatment (figure 6), confirming the results obtained by fitting of ellipsometry data (table 1). The increase of film thickness occurs not only due to the increase of the interfacial layer thickness. Since no formation of pores in the layers was observed in the TEM experiment, the expansion of the HfSiO film itself takes place due to the SiO_2 phase formation. The latter has a lower density than the HfO_2 one and can be considered as the only reason for the decrease of the density of the annealed films.

It is worth noting that the use of high-k silicate as a gate material supposes that the thickness of the gate layer can be increased in comparison with the SiO_2 gate. At the same time, as shown above, the annealing of HfSiO films at specific temperatures enables them to keep their amorphous structure without major transformation of their chemical composition. Post-deposition treatment at 1000–1100 °C results in the formation of a stable HfO_2 tetragonal phase that favors the increase of the film permittivity. The latter is considered as an advantage of the high-k gate material [5]. However, the formation of the alternating HfO_2/SiO_2 multilayer structure at 1100 °C demonstrated above could be a reason for the worsening of the dielectric properties of the films. In such a case, the use of the appropriate thickness of HfSiO material could be a solution.

4. Conclusion

Si-rich HfO_2 layers have been fabricated by RF magnetron sputtering of a HfO_2 target topped by Si chips in a pure argon plasma. The effect of the annealing treatment on the properties of the layers had been investigated by means of spectroscopic ellipsometry, x-ray diffraction, infrared absorption spectroscopy and high resolution transmission electron microscopy. It was demonstrated that annealing treatment results in the formation of an interfacial SiO_2 layer as well as in the increase of the HfSiO film thickness itself. The latter was explained by a phase separation of HfSiO into HfO_2 and SiO_2 phases over its volume. The density of the films versus annealing temperature was estimated. Its decrease with an increase of annealing temperature is explained only by a formation of SiO_2 phase over the film volume and the increase of its contribution with annealing. The formation of a HfO_2 phase was also revealed. It is shown that annealing at temperatures less than 900 °C results only in phase separation, without crystallization of the films. The higher temperature annealing favors HfO_2 crystallization into the tetragonal phase. The latter was found to be stable, offering a possibility to use such HfSiO materials for microelectronic applications, for example, for nanomemory structures with embedded Si nanoparticles requiring high temperature annealing. The formation of the multilayer Si-rich/Hf-rich structure after annealing treatment was observed and explained by surface-directed spinodal decomposition.

Acknowledgments

This work is supported by the French National Research Agency (ANR) through the Nanoscience and Nanotechnology Program (NOMAD Project no ANR-07-NANO-022-02) and, for one of the authors (LK), by the Conseil Régional de Basse Normandie through the CPER project—Nanoscience axe (2007-2013).

References

[1] Wilk G D, Wallace R M and Anthony J M 2000 *J. Appl. Phys.* **87** 484
[2] Wilk G D, Wallace R M and Anthony J M 2001 *J. Appl. Phys.* **89** 5243
[3] Goncharova L V, Dalponte M, Starodub D G, Gustafsson T, Garfunkel E, Lysaght P S, Foran B, Barnett J and Bersuker G 2006 *Appl. Phys. Lett.* **89** 044108
[4] Rignanese G-M 2005 *J. Phys.: Condens. Matter* **17** R357
[5] Fischer D and Kersch A 2008 *Appl. Phys. Lett.* **92** 012908
[6] Lee Ch-K, Lee H-S, Hwang Ch S and Han S 2008 *Phys. Rev.* B **78** 012102
[7] Cockayne A 2008 *J. Appl. Phys.* **103** 084103
[8] Tsoutsou D *et al* 2009 *J. Appl. Phys.* **106** 024107
[9] Majumder P, Jursich G and Takoudis C 2009 *J. Appl. Phys.* **105** 104106
[10] Tomida K, Kita K and Toriumi A 2006 *Appl. Phys. Lett.* **89** 142902
[11] Gourbilleau F, Khomenkova L, Dufour C, Coulon P-E and Bonafos C 2009 HfO_2-based thin films deposited by magnetron sputtering *Materials and Physics for Nonvolatile Memories* (*Mater. Res. Soc. Symp. Proc.* vol 1160) ed Y Fujisaki, R Waser, T Li and C Bonafos (Warrendale, PA: Material Research Society) pp 69–72
[12] Khomenkova L, Dufour C, Coulon P-E, Bonafos C and Gourbilleau F 2010 *Nanotechnology* **21** 095704
[13] Li W, Jia R, Chen C, Liu M, Zhu C and Long S 2009 *ECS Trans.* **18** 1071
[14] Perego M, Seguini G, Wiemer C, Fanciulli M, Coulon P-E and Bonafos C 2010 *Nanotechnology* **21** 055606
[15] Lucovsky G and Rayner G B 2000 *Appl. Phys. Lett.* **77** 2912
[16] Liu J, Wu X, Lennard W N and Landheer D 2009 *Phys. Rev.* B **80** 041403
[17] Liu J, Wu X, Lennard W N and Landheer D 2009 *ECS Trans.* **25** 163
[18] Cho M-H, Kim C Y, Moon K, Chung K B, Yim C J, Ko D-H, Sohn H C and Jeon H 2008 *J. Chem. Phys.* **129** 034705
[19] http://www.horiba.com/scientific/products/ellipsometers/software/

[20] Charvet S, Madelon R, Gourbilleau F and Rizk R 1999 *J. Appl. Phys.* **85** 4032
[21] Buiu O, Davey W, Lu Y, Mitrovic I Z and Hall S 2008 *Thin Solid Films* **517** 453
[22] Bruggeman D A G 1935 *Ann. Phys.* **416** 636
[23] Forouhi A R and Bloomer I 1986 *Phys. Rev.* B **34** 7018
[24] Jelisson G E Jr and Modine F A 1996 *Appl. Phys. Lett.* **69** 371
[25] Neumayer D A and Cartier E 2001 *J. Appl. Phys.* **90** 1801
[26] Mitrovic I Z, Buiu O, Hall S, Bungey C, Wagner T, Davey W and Lu Y 2007 *Microelectron. Reliab.* **47** 645
[27] Tan T, Liu Zh, Lu H, Liu W and Tian H 2010 *Opt. Mater.* **32** 432
[28] Kirk C T 1988 *Phys. Rev.* B **38** 1255
[29] Lange P 1989 *J. Appl. Phys.* **66** 201
[30] Ono H, Ikarashi T, Ando K and Kitano T 1998 *J. Appl. Phys.* **84** 6064
[31] Olsen J E and Shimura F 1989 *J. Appl. Phys.* **66** 1353
[32] Maunoury C *et al* 2007 *J. Appl. Phys.* **101** 034112
[33] Frank M M, Sayan S, Dörmann S, Emge T J, Wielunski L S, Garfunkel E and Chabal Y J 2004 *Mater. Sci. Eng.* B **109** 6
[34] Nguyen N V, Davydov A V, Chandler-Horowitz D and Frank M F 2005 *Appl. Phys. Lett.* **87** 192903
[35] Tang J, Zhang F, Zoogman P, Fabbri J, Chan S-W, Zhu Y, Brus L E and Steigerwald L 2005 *Adv. Funct. Mater.* **15** 1595
[36] Ho M-Y *et al* 2003 *J. Appl. Phys.* **93** 1477
[37] Monaghan S, Greer J C and Elliott S D 2005 *J. Appl. Phys.* **97** 114911